Thin Solid Films 616 (2016) 80–85

Contents lists available at ScienceDirect

Thin Solid Films

journal homepage: www.elsevier.com/locate/tsf

Enhanced Sb_2S_3 crystallisation by electric field induced silver doping

Weiling Dong [a,*], Milos Krbal [b], Janne Kalikka [a], Xin Yu Chin [c], Behrad Gholipour [c], Cesare Soci [c], P.J. Fons [d,e], Kirill V. Mitrofanov [d], Lujie Chen [a], Robert E. Simpson [a]

[a] Singapore University of Technology and Design, 8 Somapah Road, 487372, Singapore
[b] Center of Materials and Nanotechnologies (CEMNAT), Faculty of Chemical Technology, University of Pardubice, Legions Square 565, 530 02 Pardubice, Czech Republic
[c] Nanyang Technological University, 637371, Singapore
[d] Nanoelectronics Research Institute, National Institute of Advanced Industrial Science and Technology, 1-1-1 Higashi, Tsukuba 305-8565, Ibaraki, Japan
[e] SPring8, Japan Synchrotron Radiation Institute (JASRI), Kouto 1-1-1, Sayo-cho, Sayo-gun, Hyogo 679-5198, Japan

ARTICLE INFO

Article history:
Received 3 April 2016
Received in revised form 23 July 2016
Accepted 28 July 2016
Available online 2 August 2016

Keywords:
Sb_2S_3
Chalcogenide
Dissolution
Crystallisation

ABSTRACT

This work reveals that doping Ag into Sb_2S_3 substantially decreases its crystallisation temperature. We show that applying an electric field to Sb_2S_3 through Ag electrodes provides control of the crystallisation temperature and crystallisation rate. The crystal nuclei incubation time decreases substantially when the applied electric field is set to 200 kV/m. The applied electric field appears to force the Ag cations through the amorphous chalcogenide film resulting in Ag doped Sb_2S_3 filaments that extend from the cathode to the anode. This was confirmed by X-ray fluorescence composition mapping. Density functional theory molecular dynamics modelling of Ag doped Sb_2S_3 reveals that the diffusion constant of Ag is twice that of Sb or S over a wide temperature range, which implies that the Ag atoms are mobile in the amorphous Sb_2S_3 structure. The applied electric field provides a mechanism to enhance the crystallisation kinetics of Ag-doped Sb_2S_3.

1. Introduction

Amorphous Sb_2S_3 is a weakly polar semiconducting ferroelectric material with high photosensitivity and thermoelectric power [1,2], and it crystallises into an orthorhombic layered structure at a temperature that ranges from 526 K to 584 K depending on the size of the particles and the heating conditions [3]. This phase transition predominantly results from small structural changes in the coordination sphere of Sb atoms [4]. The band gap of Sb_2S_3 is dependent on the preparation conditions and can vary between 1.8 and 2.5 eV [5,6], which covers the solar spectrum. Due to the aforementioned special properties, Sb_2S_3 has been developed for a multitude of applications, such as lithium ion batteries [7–9], hydrogen storage [10,11], catalysts for Dye-Sensitized Solar Cells (DSSC) [12], photodetectors [2] and optical recording media [13].

Silver doped Sb_2S_3 exhibits a red-shifted absorption edge and consequently a reduced optical bandgap [14–18]. Its refractive index has been measured to increase by about 0.2 with silver content up to 8.2 at.% Ag [19]. Therefore, this material is attractive for potential applications in photonics. Generally, silver doped chalcogenides have found various applications in photonics and electronics. For example, silver doping has been successfully used to pattern low loss GeS waveguides using a photo-dissolution process [20]. Two-dimensional anisotropic layered Bi_2Se_3 chalcogenide nanoribbons that allow superstoichiometric intercalation of metal atoms such as Ag, Au, Co, Cu, Fe, In, Ni and Sn at the van der Waals gap of the host chalcogenide have also been investigated for potential atomic storage applications [21]. Others explored silver doped $Ge_{46}S_{54}$ thin films for use in potential programmable metallisation cell (PMC) memory devices, where the intrinsic high resistance of the device can be switched to a low resistance state by growing a stable silver electrodeposited link from the cathode to the anode. A reverse bias dissolves the electrodeposit, causing the device resistance to increase [22].

Photo-induced dissolution and diffusion of silver in chalcogenide films is a well known effect. The silver lateral diffusion process has been explained by considering the doped chalcogenide/undoped chalcogenide interface as a p-n junction. The undoped chalcogenide is modelled as p-type material whilst the doped material is n-type. The electric field of the junction pulls the Ag ions into the undoped region. As the lattice undergoes structural rearrangements caused by the photo excitation of interfacial electrons, mechanical stress is generated at the boundary arising from differences in the lattice parameters of the undoped and doped materials. This stress contributes to large structural rearrangements, including bond breaking induced formation of voids into which the silver ions can easily penetrate [23], p. 165].

We use a combination of Sb_2S_3 thin films, Ag electrodes and an electric field to enhance the crystal nucleation process in the Sb_2S_3 thin films. Ag doping in Sb_2S_3 via photo dissolution is a known effect, however, there are no reports about electric field-assisted migration of

* Corresponding author.
E-mail address: weiling_dong@mymail.sutd.edu.sg (W. Dong).

http://dx.doi.org/10.1016/j.tsf.2016.07.068
0040-6090/

Ag in Sb_2S_3. Moreover, we are not aware of any reports that suggest using silver electro-doping to enhance the crystallisation of chalcogenide materials. The objective of this work is to enhance the crystallisation kinetics of Sb_2S_3 films through electric field induced Ag doping. The effect of silver doping on the crystallisation of Sb_2S_3 is explored. The crystallisation rate, crystal growth direction and the crystallisation kinetics are altered by varying the applied electric field and temperature of the film.

2. Methods

Sb_2S_3 films were prepared on fused silica substrates by radio frequency sputtering. The chamber base pressure was 2.6×10^{-5} Pa, and the sputtering pressure was 0.5 Pa. The deposition rate was 0.43 Å/min from an Sb_2S_3 alloy target of diameter of 50.8 mm and a purity of 99.9%. Ag doped films with different silver concentration were prepared by attaching Ag pellets with different sizes on to the Sb_2S_3 target, a doping method used by other researchers [24]. The composition of the films was analysed by energy dispersive x-ray (EDX) spectroscopy in a scanning electron microscope (SEM).

The effect of silver doping on the crystallisation temperature of Sb_2S_3 was studied by measuring the crystal growth of Ag-doped Sb_2S_3 samples as a function of temperature. A microscope furnace was used to heat the films at 10 K/min in an Ar atmosphere flowing at a rate of 10 cm^3/min. The overall crystallisation temperature of the films was obtained by monitoring the intensity of the reflected light as a function of temperature. Crystallisation of Sb_2S_3 produces a large reduction in the intensity of the reflected light. The maximum rate of change in reflectivity was assumed to occur at the maximum crystallisation rate.

The force on charged particles is proportional to the external electric field, thus we expect silver cations to be electrically forced into Sb_2S_3 when a voltage is applied through Ag electrodes. We studied this effect on the crystallisation process as a function of electric field by patterning Ag electrodes, separated by a 100 μm, on the surface of Sb_2S_3 thin films using an e-beam evaporator and a shadow mask, and then applying a voltage to the Ag electrodes whilst annealing the sample in the microscope furnace.

To test the hypothesis that the electric field can influence the crystallisation temperature, a non-isothermal crystallisation study was conducted. The Sb_2S_3 films with Ag electrodes were heated from room temperature to 623 K at a rate of 2 K/min. The measurement was repeated with and without an electric field of 200 kV/m applied to the Ag electrodes.

To distinguish the influence of electric field induced Ag dissolution from that of thermal diffusion of Ag cations, isothermal crystallisation of Sb_2S_3 thin films under the influence of an external electric field was also studied. The samples were heated at a rate of 40 K/min to 493 K, equilibrated for 1 min, and then heated at 10 K/min to the measurement temperature of 513 K. At this temperature, the crystallisation was studied as a function of electric field.

We have now shown that the crystallisation temperature of Sb_2S_3 is lowered by Ag doping, and the electric field can be used to dope Ag into Sb_2S_3 from the Ag electrodes. When an electric field is applied to Ag electrodes at high temperature, both a thermal diffusion effect and an electric field induced Ag doping effect will influence the crystallisation temperature. To show this, we conducted an isothermal crystallisation study of Sb_2S_3 with and without Ag electrodes. The measurements were performed at temperatures ranging from 528 K to 548 K at 5 K intervals.

We analysed the crystallisation process of the Sb_2S_3 using microphotography. Images were collected through a 10× objective lens at a rate of one picture per second. We found that the optical contrast between the crystalline and amorphous regions was greatest when we used the "red-blue" colour channels. The "UU" image analysis tool [25] was used to determine the amorphous and crystalline areas of the film by setting an intensity threshold that was defined as $\frac{(R-B)_{crys}+(R-B)_{amor}}{2}$. Values below the threshold were considered to be amorphous whilst values above the threshold were considered to be crystalline.

The crystallisation incubation time was estimated using the generalised Johnson-Mehl-Avrami-Kolmogorov (JMAK) equation [26]:

$$x(t) = 100 - 100e^{-\frac{CI(t)U^m t^{m+1}}{m+1}} \quad (1)$$

$$I(t) = I^{ss} * \left(\frac{4\pi\tau}{t}\right)^{1/2} e^{\frac{-\pi^2\tau}{4t}} \quad (2)$$

where $x(t)$ is crystallinity as a function of time, C is the geometric factor, m is dimensionality factor, $I(t)$ is the crystal nucleation rate, U is the crystal growth rate, τ is the incubation time, and I^{ss} is the steady-state rate of nucleation of crystalline clusters.

The microscope images of the samples that were crystallised in an electric field showed filaments forming from the Ag cathode toward the anode. To establish the origin of these filaments, we performed X-ray fluorescence mapping at beam line 37XU of SPring-8, Japan. Micro-focusing optics with a nominal spot size of 100 nm were used in the scanning X-ray microprobe system. Samples of Sb_2S_3 with silver electrodes were mounted on an X-Y stage. The energy dispersive detector, which was used to measure the fluorescence signal from the sample, was placed perpendicular to the incident X-ray beam to minimise elastic scattering contributions from the sample's substrate.

Density functional theory molecular dynamics (DFT-MD) modelling was performed using the Vienna Ab-initio Simulation Package (VASP) [27], version 5.3.2, with PAW-pseudopotentials [28], PBEsol exchange-correlation functional [29], 3 fs timestep, periodic boundary conditions (PBC), and an NVT ensemble with a Nosé thermostat [30–32]. For quenching the molten model with a negative temperature ramp, a velocity rescaling algorithm was used. Energies were calculated at the Γ-point of the Brillouin zone ($\mathbf{k} = 0$).

A randomly generated structure with 60 S, 40 Sb, and 1 Ag atom was optimised by a conjugate gradient algorithm. The optimised structure was cooled from 3000 K to 1500 K in a 50 ps simulation and equilibrated at 1500 K for 20 ps to obtain a model for liquid Ag-Sb_2S_3 with 1% Ag content.

The self-diffusion constant D^* can be calculated from MD simulation trajectory as $D^* = \frac{1}{N}\sum_{i=1}^{N}\frac{(\Delta\vec{r}_i)^2}{6\Delta t}$, where $\vec{r}_i$ are the positions of the atoms 1-N, and t is the time in simulation. To study diffusion at 300–1000 K, the liquid Ag-Sb_2S_3 structure was equilibrated at each temperature, and three 15 ps simulations per temperature were performed. The diffusion constant was calculated for each run over the 15 ps trajectory, and then averaged over the three runs for each temperature. The pair distribution functions were calculated from a sample of one structure every 0.03 ps (500 structures for a 15 ps trajectory) in the three diffusion runs.

We analysed the relationship between cavities in the amorphous structure and atomic species using the pyMolDyn [33] software with 270 × 270 × 270 point domain grid (0.05 Å grid spacing) and 2.6 Å atom radius. The cavity center point was defined as the center of the largest sphere that can be placed inside the cavity.

3. Results and discussion

Ag doping significantly lowers the crystallisation temperature of Sb_2S_3 from 585 K for undoped Sb_2S_3 to 488 K with 12 at.% Ag doping. Fig. 1 shows the crystallisation temperature of the Ag-doped Sb_2S_3 films as a function of Ag content. The 2 K error bars originate from random errors associated with starting the data collection. Higher doping concentrations result in an apparent reduction in crystallisation temperature. We note that there appears to be two physical mechanisms that influence the crystallisation temperature at different silver doping

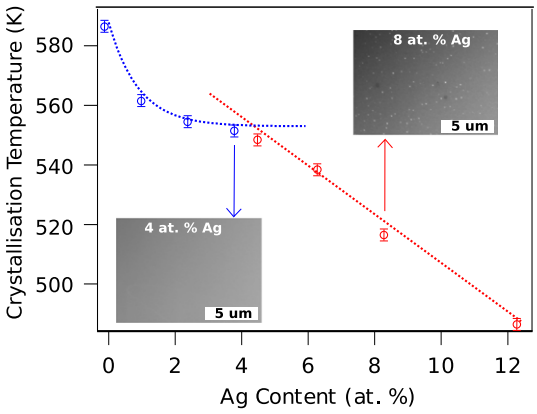

Fig. 1. Ag doped Sb_2S_3 crystallisation temperature. Inset: SEM images of sample surface for 4 at.% and 8 at.% Ag doping.

concentrations. We have fitted an exponential curve to doping concentrations lower than 4 at.% and a linear curve to the higher doping concentrations, as shown in Fig. 1. These fits are purely to guide the readers' eye and we refrain from interpreting the physical meaning of the fitting constants. However, the results clearly show that the Sb_2S_3 crystallisation temperature depends on Ag doping. It is worth noting that phase separation is observed in the as-deposited Sb_2S_3 thin films when the silver concentration is higher than 8 at.%. For lower Ag concentrations, phase separation is not observed and the as-deposited thin film appears uniform. For Ag concentrations greater than 8 at.%, Ag nanoparticles are formed on the surface of the as-deposited Sb_2S_3 film, the SEM images of 4 at.% and 8 at.% Ag doped Sb_2S_3 are shown in insets in Fig. 1. This agrees with other reports that show a limit to the concentration of Ag dissolved into chalcogenides. For example, the limit for Ag doping into $Sb_{33}S_{67}$ is ~10 at.% [23], p. 169.

A non-isothermal crystallisation study of Sb_2S_3 with Ag electrodes was conducted to test the hypothesis that the electric field can influence the crystallisation temperature. Fig. 2 shows that crystallisation begins at 557 K when there is no electric field applied to the film. However, when 200 kV/m electric field is applied, the crystallisation temperature is lowered by 22 K to 535 K. The effect of electric field on the peak crystallisation rate is compared in Fig. 2(b). At 535 K, the crystallisation rate with 200 kV/m electric field is 3.8%/s, which is substantially higher than 0.043%/s, which we measured without the electric field at the same temperature. The crystallisation temperature is lowered by the electric field, although the peak crystal growth rate is higher when no electric field is applied. This is interesting because it implies that electric field affects the nucleation rate but not the crystal growth rate. Fig. 2 indicates that with the driving force of the electric field, the Ag atoms tend to dissolute and then diffuse from one electrode to the other, substantially decreasing the crystallisation temperature. Thus we conclude that the applied electric field strongly influences the crystallisation kinetics. Furthermore, crystallisation proceeds from the cathode, which implies that the Ag cations are responsible for the electric field dependent crystallisation effect.

To measure the influence of the electric field on nucleation, an isothermal crystallisation study of Sb_2S_3 with and without Ag electrodes was conducted. As shown in Fig. 3 (a) and (c), the crystallisation rate is relatively low at 528 K, and the crystallinity is around 30% after 8060 s. The crystallisation rate is accelerated by elevating the annealing temperature to 548 K, where the film is completely crystallised after 1500 s. The peak crystal growth rate increases from 0.013%/s at 528 K to 0.16%/s at 548 K.

The electric field promotes silver dissolution into the Sb_2S_3 film, and it significantly increases the crystallisation rate. Fig. 3(b) and (d) show the influence of the electric field on the crystallisation rate of Sb_2S_3 at a constant temperature of 513 K. Increasing the applied electric field from 50 kV/m to 200 kV/m reduces the time for complete crystallisation by 79%, from 6200 s to 1300 s. To achieve a similar crystallisation rate with no electric field it would be necessary to increase the annealing temperature to 548 K. The peak crystal growth rate increases from 0.1%/s at 50 kV/m to 0.36%/s at 200 kV/m, which is more than an order of magnitude higher than that of a sample without an applied electric field at 528 K. By fitting the generalised Johnson-Mehl-Avrami-Kolmogorov (JMAK) equation [26] to the crystallinity versus time plots in Fig. 3(b), the effect of the electric field induced Ag doping on the crystal nuclei incubation time was estimated, as shown in the inset of Fig. 3(d). The length of the incubation time reflects the difficulty to initiate crystallisation. Stable crystal nuclei are required for the onset of crystal growth. As the electric field is increased, the crystallisation rate increases and the incubation time decreases, as shown in inset of Fig. 3(d). The incubation time is reduced by 75% when the applied electric field is increased from 50 kV/m to 200 kV/m. Furthermore, comparing 528 K and 0 V/m in Fig. 3(c) with an electric field of 200 kV/m at an even lower temperature of 513 K in Fig. 3(d), we see the crystallisation rate increases from 0.013%/s to 0.36%/s.

Increasing the annealing temperature or applying an electric field to the two silver electrodes accelerates the crystallisation rate. Higher temperatures provide more energy to overcome interfacial energy difference between the amorphous and crystalline phases thus result in facilitated crystal growth. Whereas the electric field increases silver content in Sb_2S_3, which creates voids in the amorphous structure. The voids accelerate the nucleation process and consequently reduce the time needed for full crystallisation. The proposed model to explain the influence of increasing temperature and applying an electric field is illustrated in Fig. 3(e).

The silver distribution in the Sb_2S_3 film between the electrodes provides evidence in support of electric field induced silver drift in Sb_2S_3. We compared X-ray fluorescence (XRF) elemental maps for samples crystallised with and without an electric field of 150 kV/m at room temperature and 513 K, see Fig. 4. With the increased temperature and

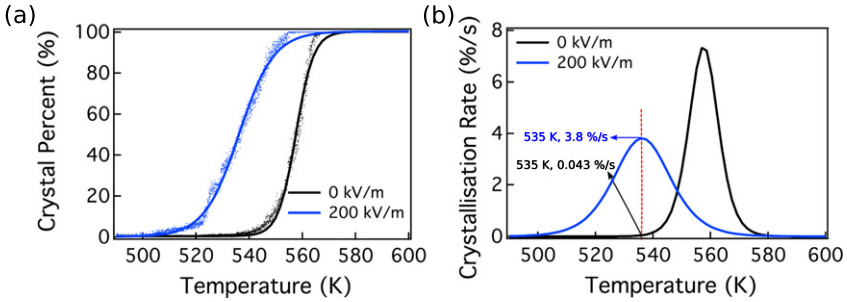

Fig. 2. (a) Crystal percentage as a function of temperature with 0 kV/m (black) and 200 kV/m (blue) applied to the Sb_2S_3 film through Ag electrodes. (b) The crystal growth rate as a function of temperature with 0 kV/m (black) and 200 kV/m (blue) applied. (For interpretation of the references to colour in this figure legend, the reader is referred to the web version of this article.)

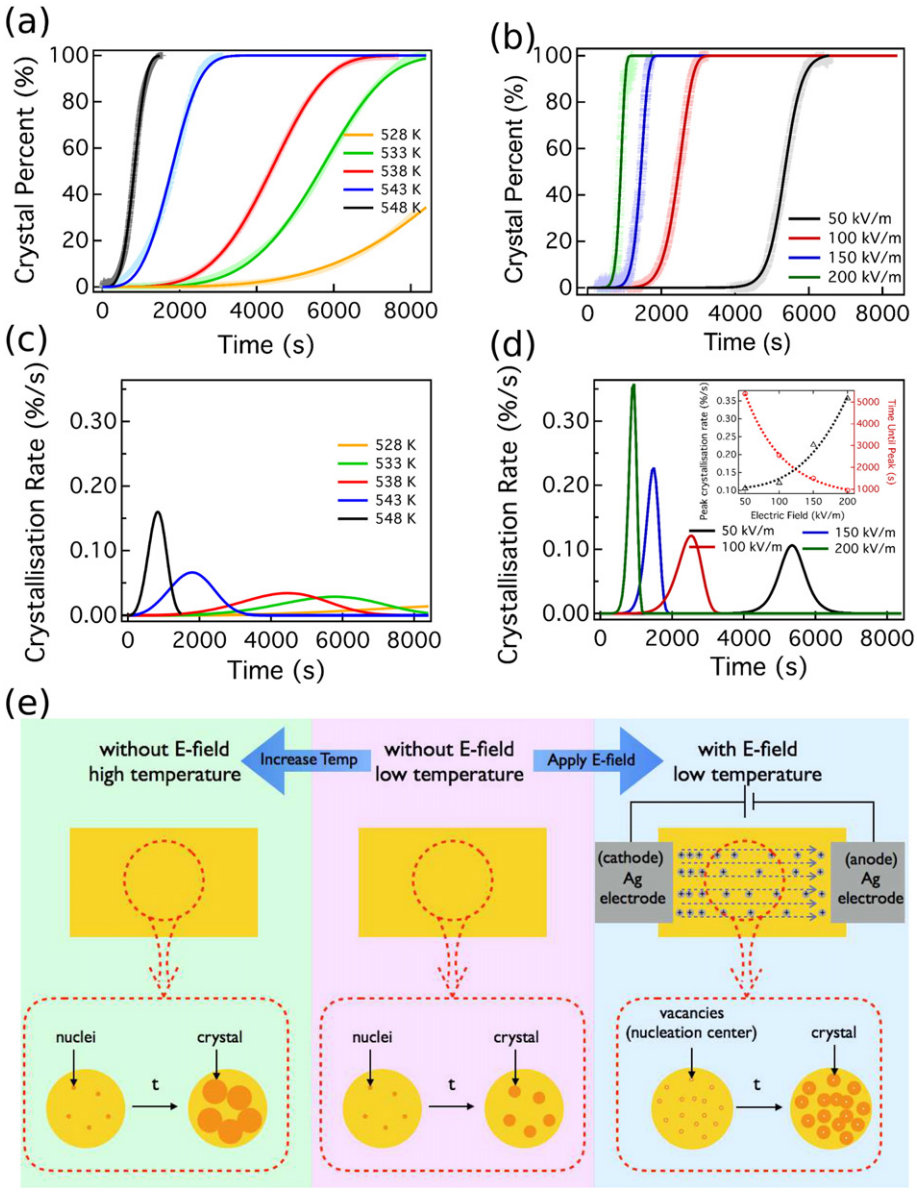

Fig. 3. Isothermal crystallisation dependence on temperature and electric field. (a) Crystallinity as a function of time for pure Sb_2S_3 films measured at different temperatures and the associated growth rate (c). For a sample held under isothermal conditions at 513 K, the effect of electric field on the crystallinity is shown in (b) and the associated growth rates are given in (d). The inset in (d) shows the crystal nuclei incubation time and the crystal growth rate as a function of electric field intensity. A model proposed to explain the electric field effect and temperature effect is given in (e). The white dots indicate the voids caused by diffusion of silver.

electric field, a silver filament can be observed between the electrodes, see Fig. 4(b). The electric field appears to enhance the drift of silver, and the effect is further enhanced at elevated temperatures.

The movement of Ag, Sb and S atoms at elevated temperatures was studied computationally with density functional theory molecular dynamics (DFT-MD) simulations. The diffusion coefficients of the three elements at different temperatures were obtained from the model, and are shown in Fig. 5(a). The diffusion constant of Ag is significantly higher than that of Sb or S, this indicates that the Ag ions are mobile in the solid amorphous Sb_2S_3 film. The optimum temperature to diffuse Ag into Sb_2S_3 is between 400 K and 500 K. The reason for this can be found from the cavity (or void) distribution around atoms of different elements. As shown in Fig. 5(b), at 300 K cavities are more common around Sb and S atoms than Ag atoms at ~2.7 Å, which is close to a typical bond length in Sb_2S_3. This can hinder Ag diffusivity as there is insufficient room around the Ag atoms. However, there is a significant number of cavities around Ag atoms at slightly longer distances close to 3.0 Å, and when the temperature is increased to 400 K, these cavities move closer to Ag atoms; the average Ag-cavity distance is shorter than S-cavity and Sb-cavity. This gives Ag atoms sufficient room to move, and increases their diffusivity in comparison to Sb and S atoms. It shows that in 600 K the cavity concentration around Ag atoms is less than around Sb or S atoms, giving further weight to the explanation, as the Ag diffusion in 600 K is lower in comparison to 500 K while Sb and S diffusivities are increasing (probably due to thermal contribution).

In conclusion, Ag doping substantially reduces the crystallisation temperature of Sb_2S_3. The Sb_2S_3 crystallisation temperature, crystallisation rate and direction, and the crystal nuclei can be enhanced by applying an electric field to Sb_2S_3 through Ag electrodes. The crystal nuclei incubation time decreases substantially when 200 kV/m is applied to the film through the Ag electrodes. X-ray fluorescence mapping shows clear Ag filament formed when an electric field is applied at elevated temperatures. The DFT-MD modelling results show that the Ag atoms are mobile in amorphous Sb_2S_3 and the optimum temperature to diffuse Ag into Sb_2S_3 is between 400 K and 500 K, due to Ag atoms locating at cavities within the amorphous network. This is in agreement with the

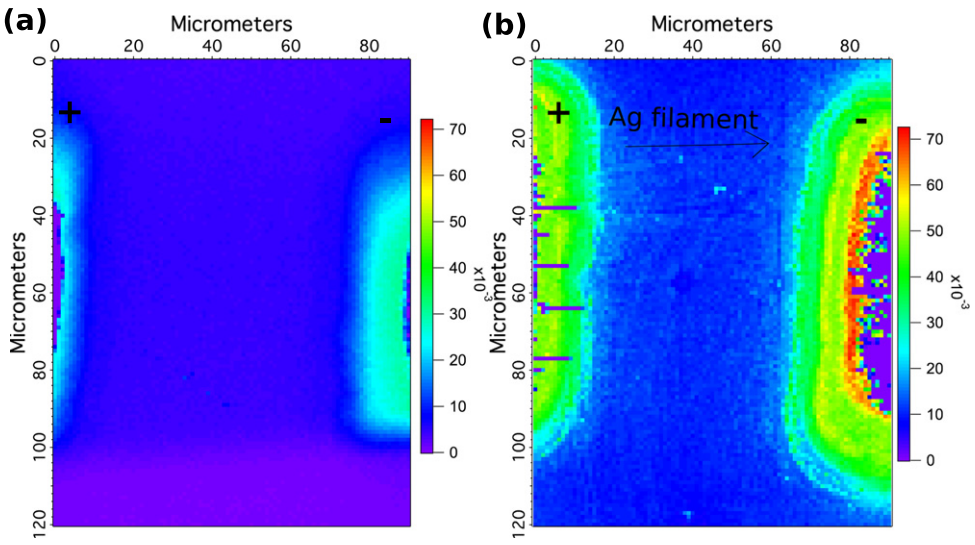

Fig. 4. Fluorescence mapping of silver on Sb_2S_3 with Ag electrodes under different temperature and electric field. Silver electrodes separation is around 75 μm, and scan area is 90 μm by 120 μm. (a) room temperature, 0 kV/m; (b) 513 K, 150 kV/m, after 30 min.

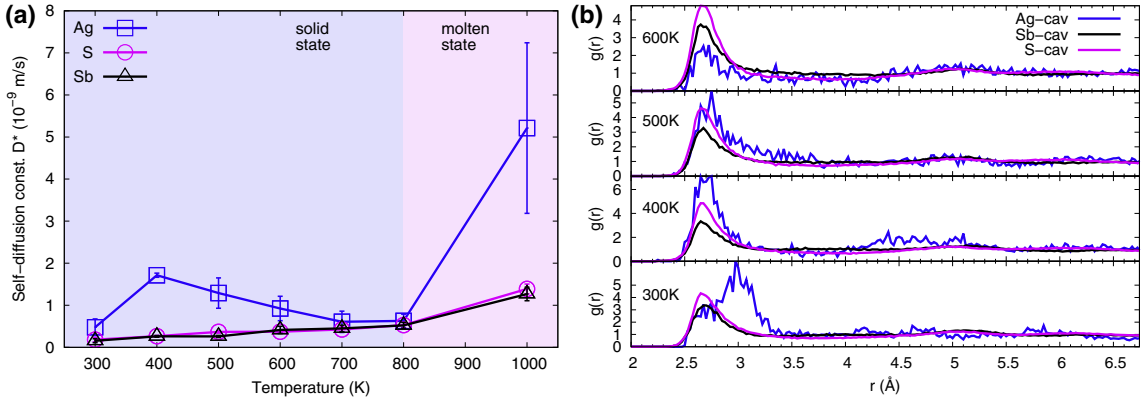

Fig. 5. Self-diffusion constant of Ag, S and Sb atoms as a function of temperature (a). Partial pair distribution functions of cavities for Ag, Sb and S atoms in DFT-MD simulations (b).

experimental results. We believe that this electric field enhanced crystallisation property could have application in non-Von Neumann logic, where the materials' electrical response is non-linear with voltage [34].

Acknowledgement

This work was supported by the SUTD International Design Center under the grant IDSF1200108OH and the Singapore Agency for Science, Technology and Research (A*STAR) funded Singapore–China joint research program under the grant 1420200046. We are grateful for beam time on BL37XU at SPring-8 (proposal 2014A1170) and the technical support of Dr. Yasuko Terada. JK is grateful for his SUTD–MIT postdoctoral fellowship. CS acknowledges support from the A*STAR (1223600007) and the Singapore Ministry of Education (MOE2011-T3-1-005). MK acknowledges support from Center of Materials and Nanotechnologies, Czech Rep, European Fund CZ.1.05/4.1.00/11.0251.

References

[1] J. Varghese, S. Barth, L. Keeney, R.W. Whatmore, J.D. Holmes, Nanoscale ferroelectric and piezoelectric properties of Sb_2S_3 nanowire arrays, Nano Lett. 12 (2) (2012) 868–872.
[2] J. Chao, B. Liang, X. Hou, Z. Liu, Z. Xie, B. Liu, W. Song, G. Chen, D. Chen, G. Shen, Selective synthesis of Sb_2S_3 nanoneedles and nanoflowers for high performance rigid and flexible photodetectors, Opt. Express 21 (11) (2013) 13639–13647.
[3] P. Pustková, Z. Zmrhalová, J. Málek, The particle size influence on crystallization kinetics of (GeS2)0.1(Sb2S3)0.9 glass, Thermochim. Acta 466 (1) (2007) 13–21.
[4] V. Rinkevichius, M. Mikalkevichius, Pyroelectric effect in antimony trisulfide single crystals, Sov. Phys. Solid State USSR 9 (10) (1967) 2360.
[5] O. Savadogo, K.C. Mandal, Studies on new chemically deposited photoconducting antimony trisulphide thin films, Sol. Energy Mater. Sol. Cells 26 (1) (1992) 117–136.
[6] S. Messina, M. Nair, P. Nair, Solar cells with Sb2S3 absorber films, Thin Solid Films 517 (7) (2009) 2503–2507.
[7] X. Zhou, L. Bai, J. Yan, S. He, Z. Lei, Solvothermal synthesis of Sb_2S_3/C composite nanorods with excellent li-storage performance, Electrochim. Acta 108 (2013) 17–21.
[8] J. Ma, X. Duan, J. Lian, T. Kim, P. Peng, X. Liu, Z. Liu, H. Li, W. Zheng, Sb_2S_3 with various nanostructures: controllable synthesis, formation mechanism, and electrochemical performance toward lithium storage, Chem. Eur. J. 16 (44) (2010) 13210–13217.
[9] P.V. Prikhodchenko, J. Gun, S. Sladkevich, A.A. Mikhaylov, O. Lev, Y.Y. Tay, S.K. Batabyal, D.Y. Yu, Conversion of hydroperoxoantimonate coated graphenes to Sb_2S_3@ graphene for a superior lithium battery anode, Chem. Mater. 24 (24) (2012) 4750–4757.
[10] C. Yan, G. Chen, R. Jin, X. Zou, H. Xu, C. Lv, Well-defined Sb_2S_3 nanostructures: citric acid-assisted synthesis, electrochemical hydrogen storage properties, Cryst. Res. Technol. 48 (8) (2013) 566–573.
[11] F. Cao, W. Liu, L. Zhou, R. Deng, S. Song, S. Wang, S. Su, H. Zhang, Well-defined Sb_2S_3 microspheres: High-yield synthesis, characterization, their optical and electrochemical hydrogen storage properties, Solid State Sci. 13 (6) (2011) 1226–1231.
[12] H. Zhang, M. Ge, L. Yang, Z. Zhou, W. Chen, Q. Li, L. Liu, Synthesis and catalytic properties of Sb_2S_3 nanowire bundles as counter electrodes for dye-sensitized solar cells, J. Phys. Chem. C 117 (20) (2013) 10285–10290.

[13] S. Shaji, A. Arato, J. O'Brien, J. Liu, G.A. Castillo, M.M. Palma, T.D. Roy, B. Krishnan, Chemically deposited Sb_2S_3 thin films for optical recording, J. Phys. D. Appl. Phys. 43 (7) (2010) 075404.
[14] T. Wagner, G. Dale, P. Ewen, A. Owen, V. Perina, Kinetics of the thermally and photoinduced solid state reaction of Ag with as33s67 films, J. Appl. Phys. 87 (11) (2000) 7758–7767.
[15] T. Wagner, Photo-and thermally-induced diffusion and dissolution of Ag in chalcogenide glasses thin films, J. Optoelectron. Adv. Mater. 4 (3) (2002) 717–727.
[16] T. Wagner, S. Kasap, M. Vlček, M. Frumar, P. Nesladek, M. Vlček, The preparation of the Agx(As033S0.67)100-x amorphous films by optically-induced solid state reaction and the films properties, Appl. Surf. Sci. 175 (2001) 117–122.
[17] T. Wágner, J. Gutwirth, M. Krbal, M. Vlček, M. Vlček, M. Frumar, Ag-Sb-S amorphous chalcogenide thin films prepared by optically induced dissolution and diffusion of silver, J. Non-Cryst. Solids 326 (2003) 238–242.
[18] M. Vl, Physical properties and structure of amorphous Agx (Sb033S0.67)100-x prepared by optically-induced diffusion and dissolution of silver into spin-coated amorphous Sb33S67 films and their application for optical recording, J. Optoelectron. Adv. Mater. 5 (5) (2003) 1139–1146.
[19] T. Kosa, R. Rangel-Rojo, E. Hajto, P. Ewen, A. Owen, A. Kar, B. Wherrett, Nonlinear optical properties of silver-doped As_2S_3, J. Non-Cryst. Solids 164 (1993) 1219–1222.
[20] C. Huang, D. Hewak, Silver-doped germanium sulphide glass channel waveguides fabricated by chemical vapour deposition and photo-dissolution process, Thin Solid Films 500 (1) (2006) 247–251.
[21] K.J. Koski, C.D. Wessells, B.W. Reed, J.J. Cha, D. Kong, Y. Cui, Chemical intercalation of zerovalent metals into 2d layered Bi_2Se_3 nanoribbons, J. Am. Chem. Soc. 134 (33) (2012) 13773–13779.
[22] M. Mitkova, Y. Sakaguchi, D. Tenne, S.K. Bhagat, T.L. Alford, Structural details of ge-rich and silver-doped chalcogenide glasses for nanoionic nonvolatile memory, Phys. Stat. Solidi A 207 (3) (2010) 621–626.
[23] A.V. Kolobov, Photo-Induced Metastability in Amorphous Semiconductors, John Wiley & Sons, 2006.
[24] Y. Sato, H. Akizuki, T. Kamiyama, Y. Shigesato, Transparent conductive nb-doped TiO_2 films deposited by direct-current magnetron sputtering using a TiO_2-x target, Thin Solid Films 516 (17) (2008) 5758–5762.
[25] L. Chen, An image-processing software package: Uu and fig for optical metrology applications, in: International Conference on Optics in Precision Engineering and Nanotechnology (icOPEN2013), Int. Soc. Opt. Photonics (2013) 87690U.
[26] S. Senkader, C. Wright, Models for phase-change of Ge2Sb2Te5 in optical and electrical memory devices, J. Appl. Phys. 95 (2) (2004) 504–511.
[27] G. Kresse, J. Hafner, Ab initio molecular dynamics for open-shell transition metals, Phys. Rev. B 48 (17) (1993) 13115.
[28] G. Kresse, D. Joubert, From ultrasoft pseudopotentials to the projector augmented-wave method, Phys. Rev. B 59 (3) (1999) 1758.
[29] J.P. Perdew, A. Ruzsinszky, G.I. Csonka, O.A. Vydrov, G.E. Scuseria, L.A. Constantin, X. Zhou, K. Burke, Restoring the density-gradient expansion for exchange in solids and surfaces, Phys. Rev. Lett. 100 (13) (2008) 136406.
[30] S. Nosé, A unified formulation of the constant temperature molecular dynamics methods, J. Chem. Phys. 81 (1) (1984) 511–519.
[31] N. Shuichi, Constant temperature molecular dynamics methods, Prog. Theor. Phys. Supp. 103 (1991) 1–46.
[32] D. Bylander, L. Kleinman, Energy fluctuations induced by the nosé thermostat, Phys. Rev. B 46 (21) (1992) 13756.
[33] J. Kalikka, J. Akola, R. Jones, Simulation of crystallization in Ge2Sb2Te5: a memory effect in the canonical phase-change material, Phys. Rev. B 90 (18) (2014) 184109.
[34] T. Ohno, T. Hasegawa, T. Tsuruoka, K. Terabe, J.K. Gimzewski, M. Aono, Short-term plasticity and long-term potentiation mimicked in single inorganic synapses, Nat. Mater. 10 (8) (2011) 591–595.